Development of a High-Throughput Assay for Directed Evolution of Polypropylene-Degrading Enzyme HIS1

Introduction

Polypropylene (PP) accounts for 14% of global polymer production; however, its recycling rate remains below 1% (Nordahl et al., 2023). 60% of manufactured plastics are discarded, accumulating in landfills and the environment (Geyer et al., 2017). While plastic degradation has largely focused on easily hydrolysable polymers like polyethylene terephthalate (PET), PP remains a challenge due to its non-hydrolysable backbone and high crystallinity (Wang et al., 2024). The chemical structure of PP containing covalent bonds $[CH_3CH_6]_n$, makes it highly resistant to enzymatic attack. Degradation of PP is mainly facilitated through abiotic processes, initiated by UV cleavage of C-H bonds (Fig. 1A). This triggers radical chain reactions that generate hydroperoxides, drive β-scission, and release oxygenated fragments such as ketones, aldehydes, and olefins (Fig. 1A).

Most recently, a promiscuous enzyme has been found to cause notable degradation of PP through hydroxylation; Tan et al performed a metagenomic screen looking for bioremediation enzyme sequences leading to the discovery of HIS1, a protein found in *Oryza sativa japonica* encoding the Fe(II)/2-oxoglutarate-dependent oxygenase. Such enzymes employ a conserved 2-His-1-carboxylate facial triad to activate O_2, generating a high-valent Fe(IV)=O intermediate, and abstract hydrogen atoms from otherwise inert C–H bonds before hydroxylation (Martinez and Hausinger, 2015) (Fig. 1B). HIS1 confers resistance to multiple β-triketone herbicides (baths), such as benzobicylon (BBC), by catalysing their hydroxylation, which neutralises their 4-Hydroxyphenylpyruvate Dioxygenase (HPPD)-targeting herbicidal activity (Maeda et al., 2019). HIS1 is shown to detoxify a wide range of structurally related bTHs demonstrating its substrate promiscuity. This broad-range specificity leads to its proposed ability to also act as a PPase through hydroxylation of the polymer.

Directed evolution (Delgado et al., 2019) is a powerful method of improving biomolecule properties that mimics natural evolution. It involves iterative cycles of generating genetic diversity, typically through site-directed or random mutagenesis, and screening libraries of mutants for target traits (Wang et al., 2021). We aimed to use a combination of site-directed and combinatorial mutagenesis to target surface-exposed residues of HIS1 for mutation; we hypothesized that mutations to increase hydrophobicity at these target residues would increase the affinity of the enzyme to the surface of PP due to increased hydrophobic interactions. The challenge of working with DE for PP degradation is the lack of an existing high throughput assay to detect such changes. This has created a bottleneck in the research; consequently, an integral part of this project is to generate a novel screen for the mutant library. Therefore, the overall aim of this project is to simultaneously design a mutant library and a high throughput screen for the testing of our library. The screen relies on detecting functional groups produced from oxidation of the polymer which could make it a useful tool for other DE projects relating to the degradation of plastics with similar structures to PP.

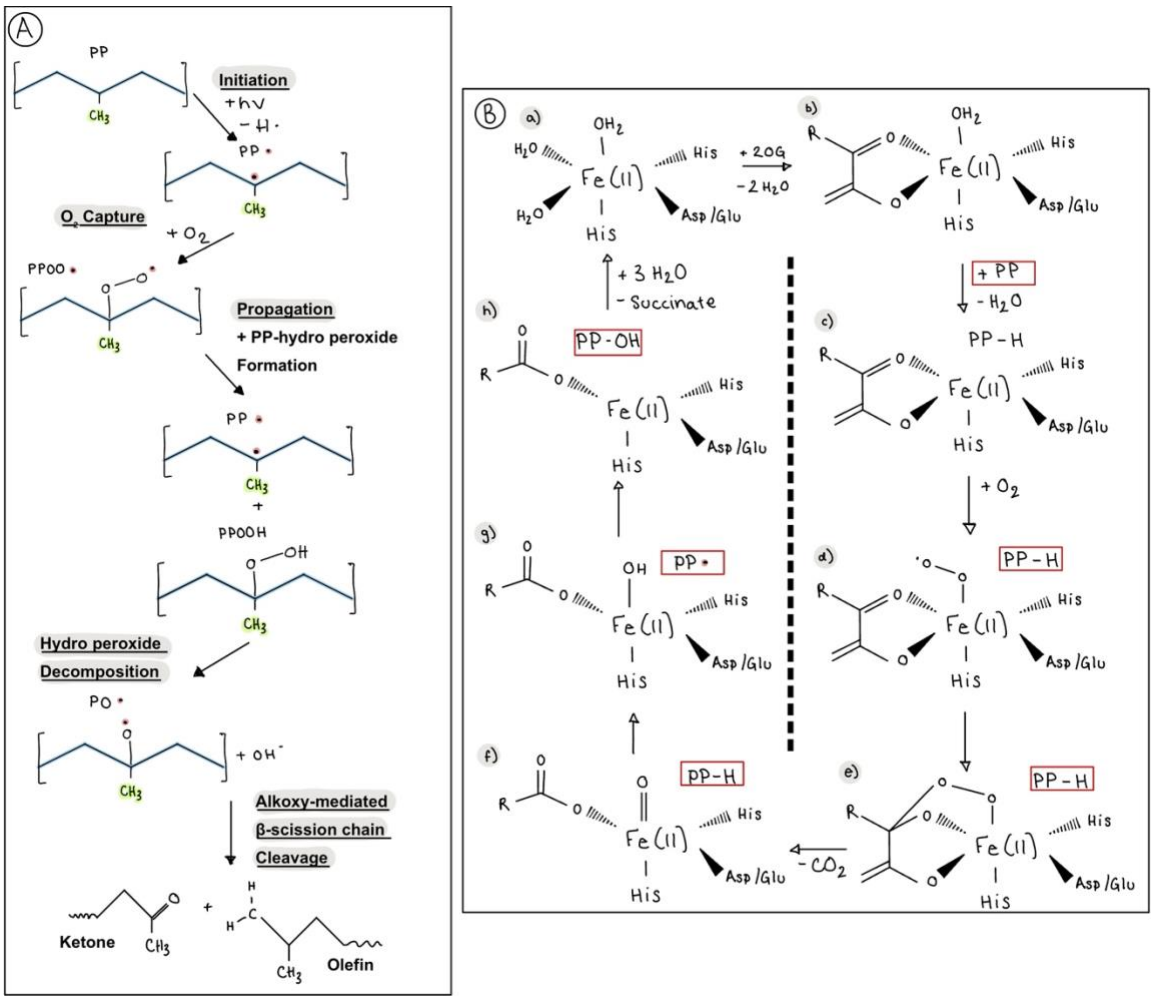

Figure 1. Chemical representation of PP breakdown. (A) *Abiotic degradation of PP*. Initiation: UV light (hv) induces C-H bond cleavage generating a radical (PP·). O_2 Capture: Radicals react quickly with oxygen to form peroxy radicals (PPOO·). Propagation: Peroxy radicals abstract H from neighbouring chains, producing hydroperoxides (PPOOH) and regenerating radicals, feeding the chain reaction. Hydroperoxide decomposition: PPOOH decomposes into Alkoxy (PPO·) and hydroxyl (HO·) radicals. Chain cleavage: Alkoxy radicals undergo ß-scission, yielding oxygenated fragments (ketones, aldehydes, alcohols, acids) and unsaturated species (olefins). ***(B)*** *Overview of the catalytic mechanism of HIS1***.** a) Fe(II) is coordinated by the 2-His-1-carboxylate triad and 3 water molecules. b) 2-OG binds bidentately, displacing two water molecules. c) binding of PP displaces the final water, opening a site for O_2 binding. d-e) O_2 forms an Fe(III)-superoxo intermediate, which attacks 2-OG to give a peroxo-hemiketal. f) Oxidative decarboxylation of 2-OG, releases C and forming a high valent Fe(IV)=O (ferryl) species with succinate bound. g) The ferryl species abstracts an H atom from PP, generating a radical (PP·) and Fe(III)-OH. h) In the canonical pathway, radical rebound produces the hydroxylates product, which dissociates to complete the cycle. Figures adapted from (Gewert et al., 2015)and (Martinez and Hausinger, 2015)

Results

Directed Evolution

Computational Analysis and Target Site Selection

Molecular dynamics and docking simulations with PP were conducted on HIS1 to identify target residues for mutation (Fig. 3A). The proposed active site residues for HIS1 (Fig.3C) indicates a small pocket for substrate interactions; given that PP is a large polymeric ligand, it was hypothesized that increasing the hydrophobicity of surface exposed residues could expand the interaction interface, resulting in higher binding affinity to PP (Wang et al., 2024). Due to screening capacities and time restraints, we identified the degenerate codon DTN to be optimal for our experiments, as it yields an array of four hydrophobic residues (I, V, L, and F), and a stop codon. Shortlisted residues were screened via FoldX for mutational stability (Delgado et al., 2019). All shortlisted candidate residues and their average ΔΔG values across all 4 possible mutations were calculated (Fig. 2). Candidate residues were screened using a threshold value of -0.15, resulting in a final list of seven target sites: N110, E148, D268, A297, D304, E305, and D307 (Fig. 3B).

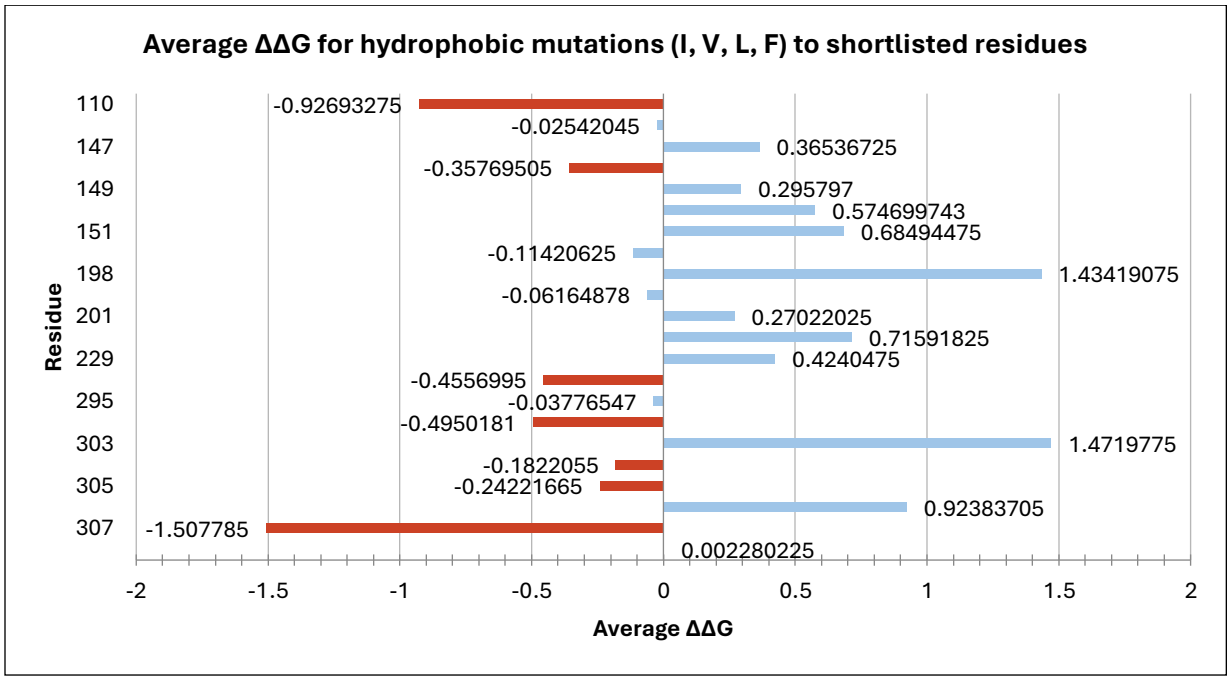

Figure 2: Average ΔΔG of shortlisted residues. ΔΔG was calculated for all four hydrophobic residues encoded by the degenerate codon DTN before an average value was calculated. Targets selected for mutation are highlighted in red. Selection was conducted using a threshold value of -0.15. ΔΔG is the measure of the change in protein folding free energy, where $\Delta\Delta G = \Delta G_{Mutant} - \Delta G_{WT}$; a positive value means the mutation could destabilise the protein, whereas a negative value means the mutation could stabilise the structure (Yamamoto et al., 2023, Buss et al., 2018)

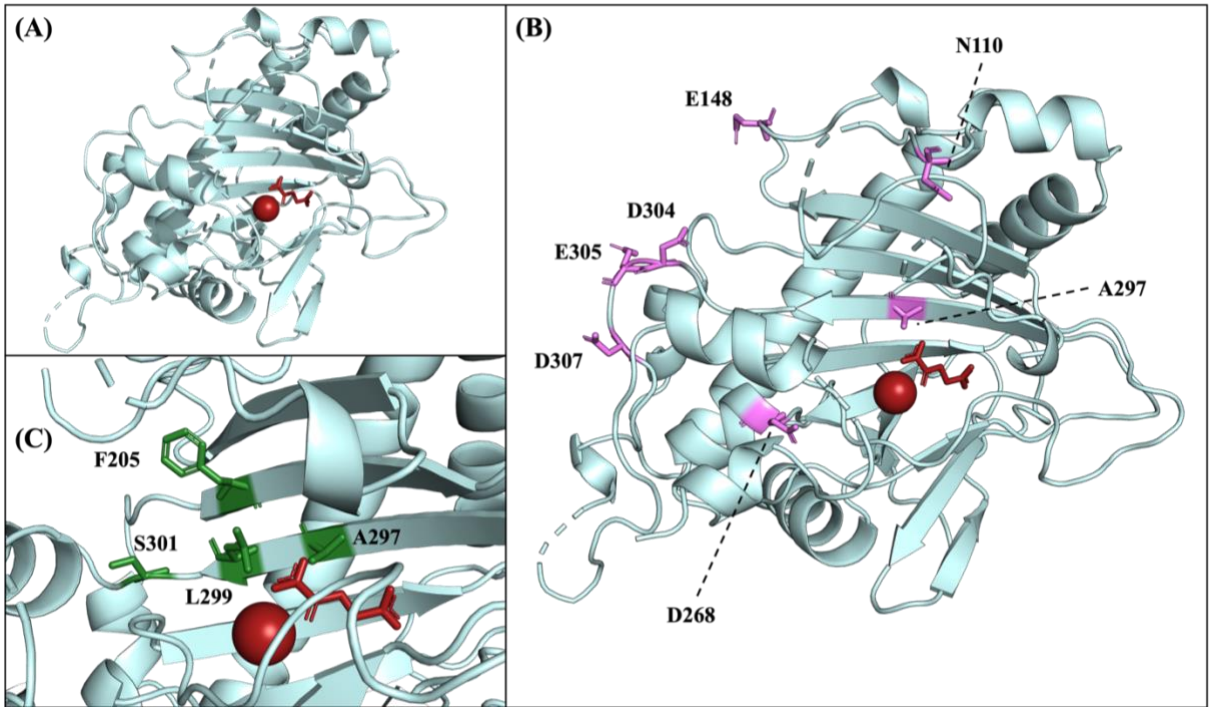

Figure 3. HIS1 structure with co-factors Fe^{2+} and 2-OG highlighted in red. **(A)** Structure of HIS1 adapted from PDB: 8y4u. Positioning of 2-OG was derived from alignment with PDB: 8s7b. **(B)** Target residues were identified through computational analyses and are highlighted in pink. The degenerate codon DTN was used to substitute these residues with more hydrophobic (I, V, L, or F) residues. **(C)** The proposed active site of HIS1 (Wang et al., 2024). The 4 residues highlighted in green are proposed to interact with the substrate.

Library Generation

To efficiently minimize library size, a dual screen approach was adapted. Mutants would initially be generated through single-site-directed mutagenesis and screened for neutral or positive effects. This would be followed by a combinatorial mutagenesis phase combining the mutants from the previous screen. To generate site-directed mutations, we adapted a protocol for combinatorial library generation to create single-site mutants (Sadler et al., 2018). This strategy was chosen as it would facilitate both single-site and combinatorial mutagenesis.

To verify the efficacy of this strategy, the single-site mutant of N110 was synthesized and sequenced (Methods C.1.2.2). Initial asymmetric PCR attempts yielded no product. The original protocol (Sadler et al., 2018) was modified by adjusting the primer ratio and extension time from 20:1 and 30 seconds to 100:1 and 60 seconds, resulting in bands of the correct size (700bp) (Fig. 4).

Initial attempts to generate full-length PCR products did not yield product. This was most likely due to low single-stranded mutant megaprimer concentration (5.8 ng/µL); increasing the concentration to 63 ng/µL by pooling six 50µL asymmetric PCR products resulted in low levels of full-length gene (Fig. 4B). Ligation, transformation, and culturing did not work at backbone concentrations of 2.7 ng/µL but succeeded at 33 ng/µL.

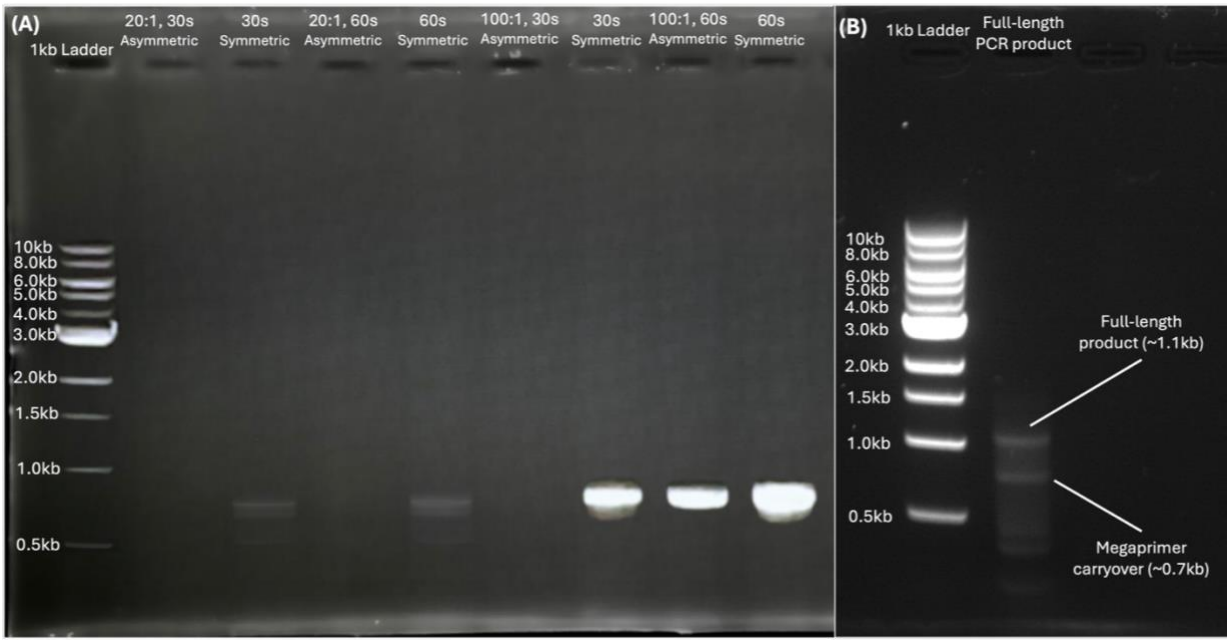

Figure 4: Gel electrophoresis of asymmetric and full-length PCR products. (A) Gel electrophoresis of asymmetric (test sample) and symmetric (control) PCRs to generate mutant megaprimers. Gel Ratios (20:1, 100:1) refer to ratios between non-mutagenic reverse primers and mutagenic forward primers. Time (30s, 60s) refers to extension time for PCR thermocycles. Asymmetric PCR products were only observed for the 100:1, 60s sample. (B) Gel electrophoresis of full-length PCR product. Full length PCR product was observed at low levels alongside megaprimers carried over from the PCR reaction.

A heterogeneous liquid culture and six plated colony samples were sent for Sanger sequencing to confirm the presence of mutations at residue 110. The liquid culture sample should have contained a library of different mutations at site 110; however, this was not confirmed, as the DNA concentration was too low, resulting in inaccurate sequencing. Colony samples were fully sequenced, showing that the gene insert was present; however, the intended mutation was not incorporated (Fig. 5). Library generation was subsequently halted due to delayed screen optimization.

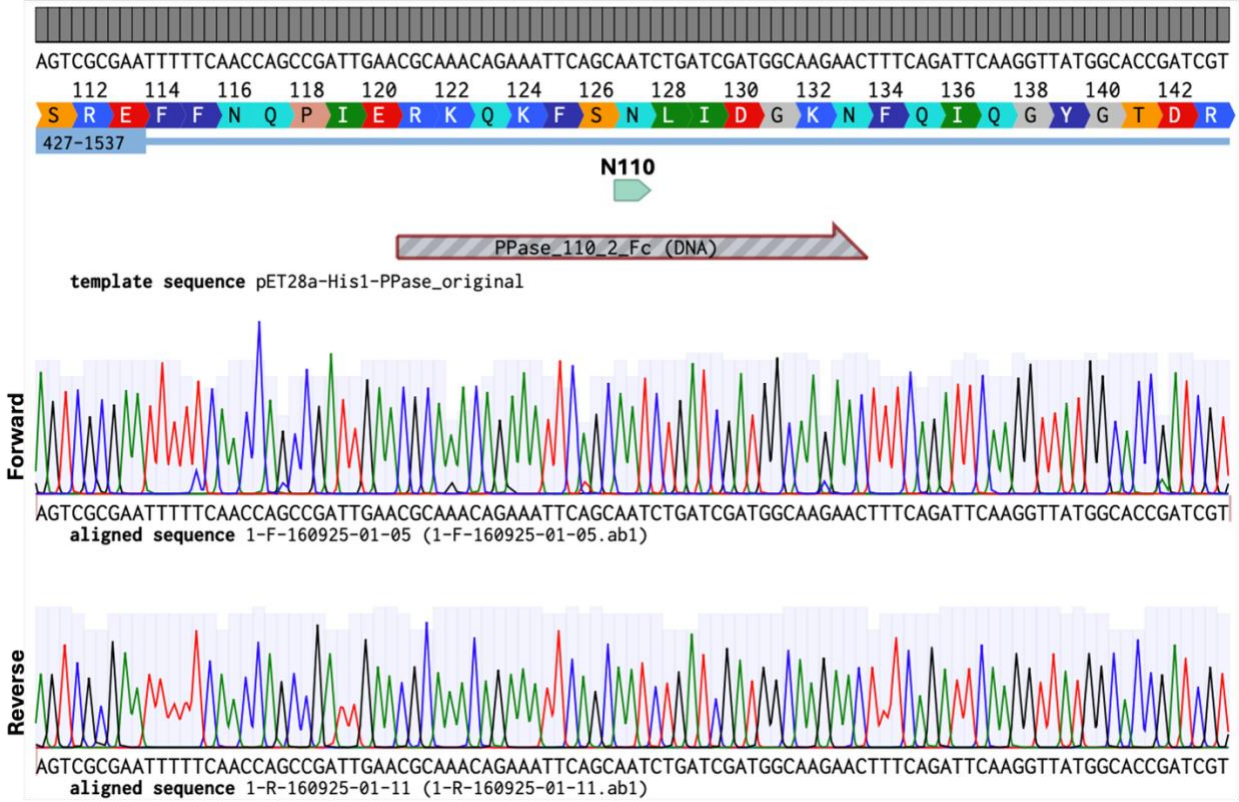

Figure 5: Representative alignment of sequenced colony against unmutated pET28a-His1 plasmid. The top aligned sequence is the forward sequencing data, and the bottom aligned sequence is the reverse sequencing data. Residue N110 is highlighted above in green. No bases in the aligned sequences have been highlighted in red, indicating that the mutation has not been incorporated. All 6 colonies sent for sequencing showed similar results.

Evaluation of Enzymatic Activity

Alongside the development of our high-throughput assay, various tests were used to assess the activity of HIS1 in both lysate and purified form. TLC was used to assess HIS1 activity on 4-hydroxyphenylpyruvate (HPP). GC-MS was used to test for breakdown products are in solution. Alternatively, AFM and FTIR were used to look for evidence of oxidation on the plastic surface as indicators of enzymatic activity. Tubes were treated in 3-day intervals. The solutions were exchanged every 24 hours with appropriate replacement of co-factors and fresh lysate or pure HIS1 solution.

TLC analysis for assessing HIS1 activity

Thin-layer chromatography (TLC) was used to assess the activity of HIS1 lysate and purified HIS1 on 4-hydroxyphenylpyruvate (HPP), with an empty vector (Li et al., 2018) lysate and HEPES serving as controls, respectively. Previous work using HPLC had shown that

purified HIS1 can reduce HPP levels (Sadler lab, unpublished data). We aimed to replicate this observation using TLC.

TLC analysis (n=3) of reaction mixtures containing either HIS1 or EV lysate, with or without HPP were performed (Fig. 6A). The Rf values for HPP were consistent across experiments, with two distinct spots observed: one at Rf = 0.72, 0.76, 0.77 (likely representing the enol form of HPP) and another at Rf = 0.54, 0.62, 0.61 (likely representing the keto form). Purified HIS1 samples produced a single spot at Rf = 0.72, 0.70, 0.68, which was identical to the HEPES control (Fig. 6B).

Importantly, the HIS1 + HPP/Pure HIS1 + HPP samples displayed the same Rf profile as the controls, with no loss of HPP signal or appearance of additional products (Fig.6A, 6B). These findings indicate that, under the conditions tested, both forms of HIS1 (lysate and purified) exhibited no detectable activity on HPP.

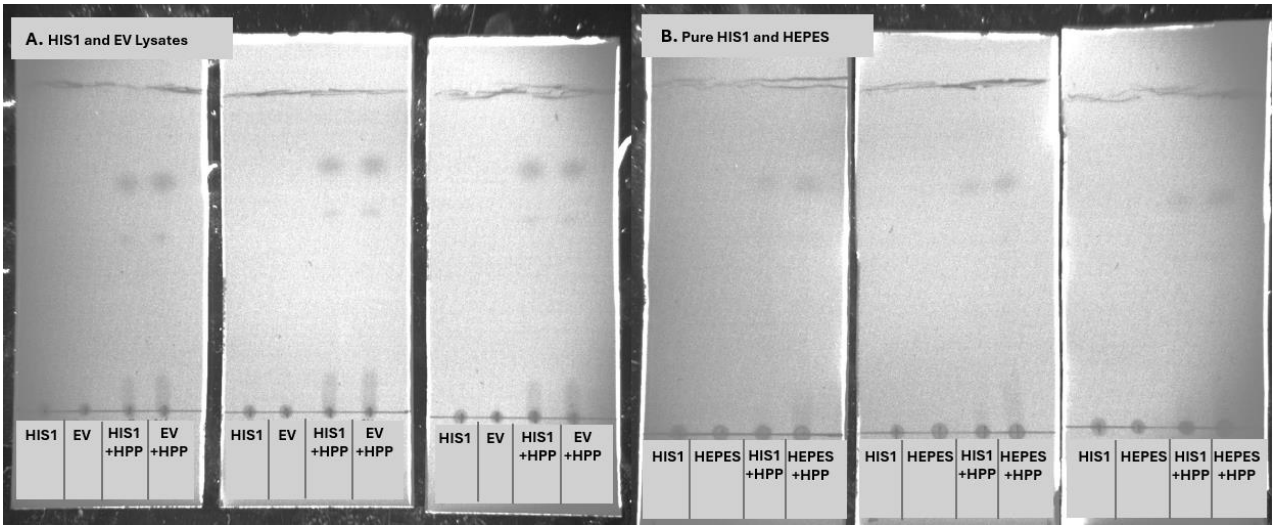

Figure 6. TLC analysis of HPP breakdown with HIS1 lysate (A) and purified HIS1 (B). (A) Reaction mixtures contained HIS1 lysate, empty vector (Li et al.) lysate, HIS1 + HPP, or EV + HPP. For each condition, samples were spotted in triplicates across 3 TLC plates. HPP consistently migrated as two species, with Rf values of 0.72/0.54 labelled (Plate 1), 0.76/0.62 (Plate 2), and 0.77/0.61 (Plate 3). No differences were observed between HIS1 and EV samples, indicating undetectable HIS1 activity under these conditions. **(B)** Reaction mixtures contained Pure HIS1, HEPES, Pure HIS1 + HPP, or HEPES + HPP. The same method as (A) was used, giving Rf values of 0.72 (Plate 1), 0.70 (Plate 2), and 0.68 (Plate 3). No differences were observed between Pure HIS1 and HEPES samples.

Gas Chromatography-Mass Spectrometry (GC-MS)

GC-MS was performed on the Pure HIS1-treated PP films to investigate for potential breakdown products in solution. The chromatograms of both untreated and HIS1-treated

samples showed similar profiles with minor differences in peak intensity (Fig. 7A). The major peak in both samples was identified as 9-Octadecenamide at approximately 21.2-21.4 minutes acquisition time (Fig. 7B). At 21.5 minutes the observed peak decreases minorly between the untreated and the sample (Fig. 7B). In addition, a peak shown at 26.5 minutes in the control is not seen in the sample (Fig 7A).

No expected oxidation products, including: 2-Pentene, Undecane, Dodecane, 3-Methyl-5-propylnonane, 2,6,10-Trimethyltridecane, and 2,6,10,14-Tetramethylpentadecane (Tan et al., 2024) were seen in the sample TIC. 9-Octadecenamide peaks in both samples have comparable intensities, suggesting it is not a product of enzymatic breakdown, but a contaminant or a product of previous treatment during manufacturing. It is worth considering the possibility that the use of dichloromethane for compound extraction can exclude some of the more polar compounds that may be in solution. Another limitation to note is that a large proportion of oxidation products may remain bound to the surface of the plastic with few to no products in solution. Indicating that GC-MS isn't an accurate representation of the full oxidative profile. Consequently, both Atomic Force Microscopy and Fourier Transform Infrared spectroscopy were conducted to provide a better understanding of any surface chemical changes.

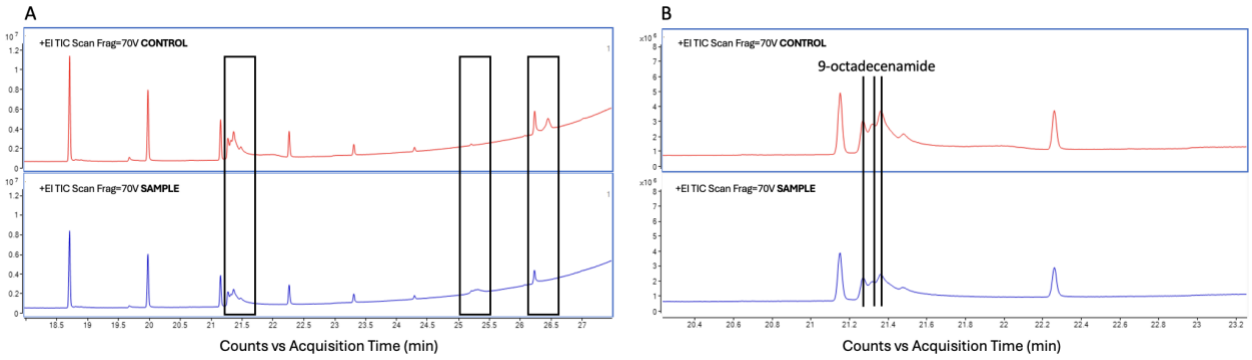

Figure 7. GC-MS total ion chromatograms (TIC) for Pure HIS1-Treated and Untreated Polypropylene Samples. **(A)** Overview chromatograms showing major peaks of control (red) and sample (blue). The black boxes denote areas where peaks have appeared, disappeared or changed in intensity between the sample and control. **(B)** Detailed view with integrated peak areas for quantitative analysis. 9-octadecenamide identified as a peak in both control and sample. GC-MS performed at EdinOmics and figures made by Dr Tessa Moses.

Atomic Force Microscopy (AFM)

Samples sent for AFM study (1 μm and 10 μm scales) were treated with HEPES buffer, Pure HIS1 protein, HIS1 lysate, and EV lysate. They were compared with untreated and HEPES buffer treated samples (negative control). Biological triplicates of each sample were sent over for AFM analysis and consistent data was obtained between triplicates (Fig. S7). Roughness measurements were taken across all samples (Fig. 8; Table S3; Table S5). No significant differences were observed between HEPES-treated and untreated samples (10 μm scan, $p=0.07$; 1 μm scan, $p=0.50$) (Fig. 8). Pure HIS1-treated samples demonstrated a significant increase in roughness values across both 10 μm ($p=0.0029$) and 1 μm ($p= 0.0012$) scans, compared to untreated samples (Fig. 8). However, HIS1 lysate-treated samples demonstrate no difference to untreated controls across both 10 μm ($p=0.14$) and 1 μm ($p=0.27$) scans while EV lysate presents as significantly different to untreated samples in 1 μm ($p=0.01$) scans (Fig. 8). Images of 10 μm scans show evidence of a protein coating in the EV lysate explaining the significantly increased roughness values (Fig. S6).

In 1 μm scans, particulate matter on the sample surface was avoided wherever possible to more accurately represent the material surface after degradation (Fig. 9). The difference between pure HIS1-treated and untreated samples were visualised in their scans and 3D terrains, with notably more drastic features on the pure HIS1-treated sample (Fig. 9). The HIS1 lysate-treated sample does not demonstrate remarkably different features in comparison to the untreated sample (Fig. 9). The 3D terrain of the EV lysate-treated sample (Fig. 9) seems affected by a protein coating or particulate matter induced by insufficient washing.

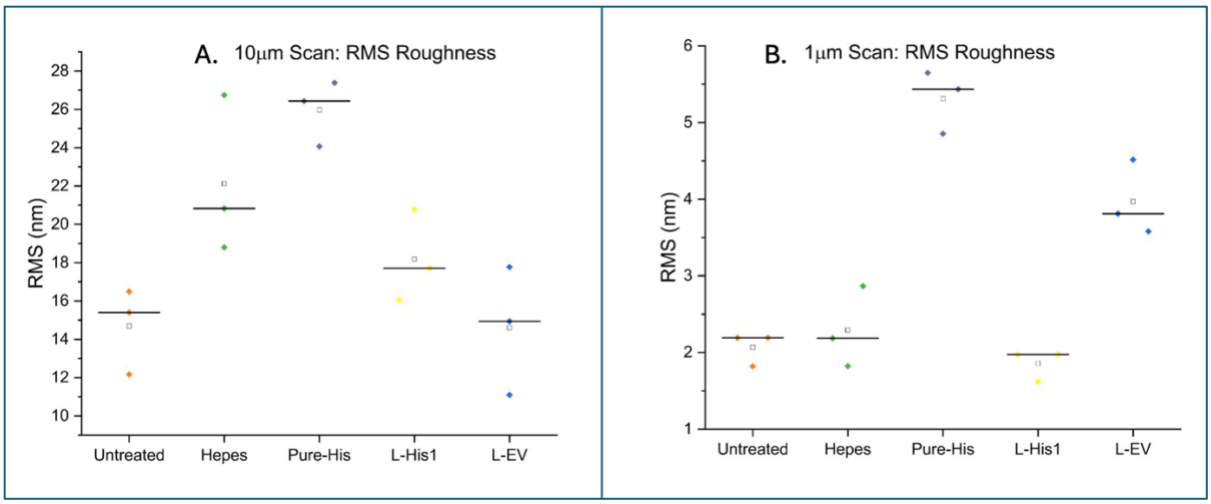

Figure 8. Average roughness of (A) 10 µm and (B) 1 µm scans. Roughness values provided by the microscope are compiled by Dr. Laura Charlton. Root Mean Square (RMS) of each roughness values were calculated and shown along the y-axis in nanometres. Along the x-axis, are the list of samples measured. 'Untreated' is the negative control sample of just the PP film; each orange diamond denotes the root mean squared of each sample in the triplicate. 'Hepes' is the PP film treated in HEPES buffer; each green diamond indicates the root mean squared of each sample in the triplicate. 'Pure-His' is the PP film treated with the purified HIS1 enzyme; each purple diamond represents the root mean squared of each sample in the triplicate. 'L-His1' is the PP film treated with the HIS1 lysate; each yellow diamond point is the root mean squared of each sample in the triplicate. 'L-EV' is the PP film treated with the empty vector (Li et al., 2018) lysate; each blue diamond points is the root mean squared of each sample in the triplicate. White squares shows the averages of each triplicate's RMS. Detailed able of values are indicated in the Supplementary Table 3 and 5.

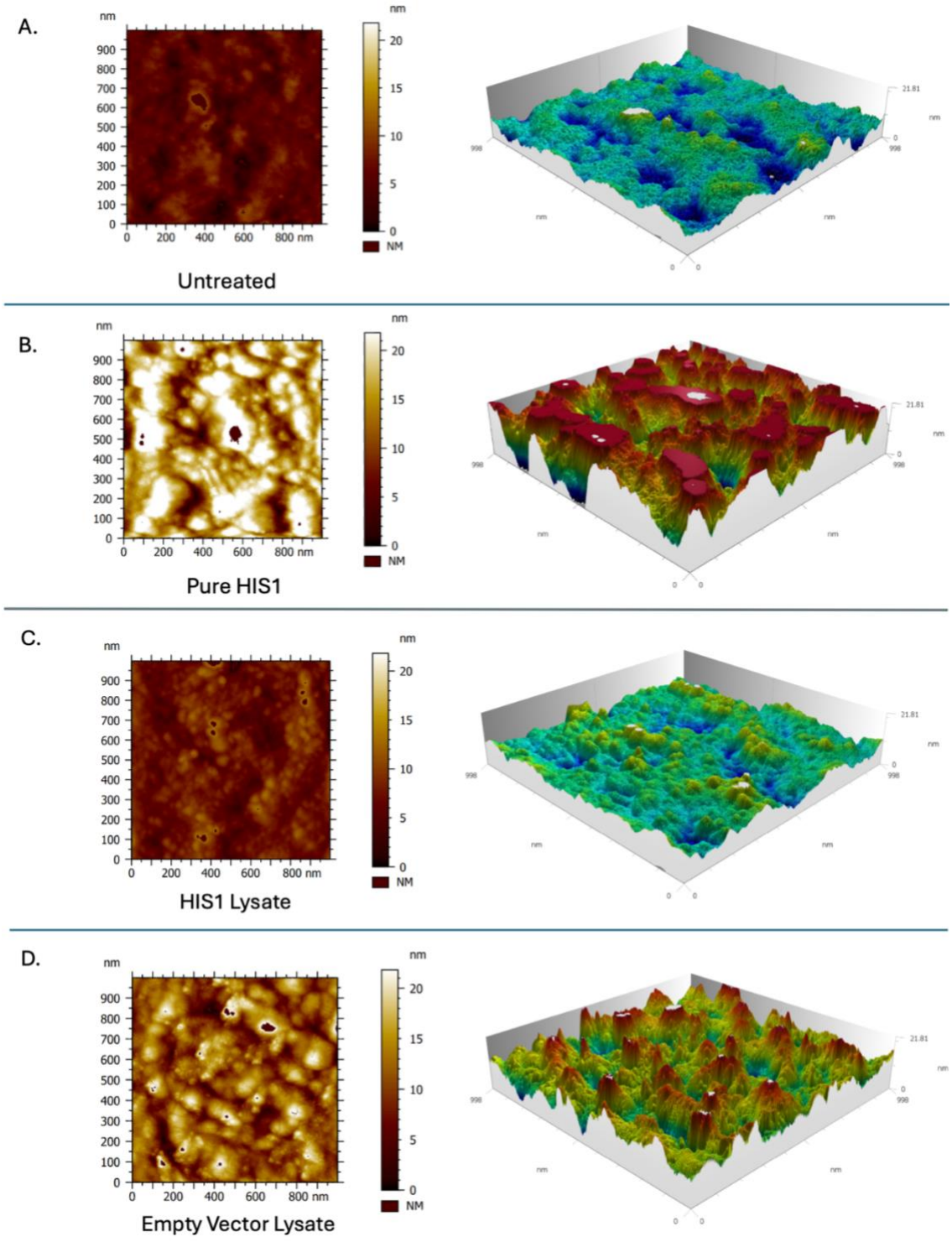

Figure 9. 1 µm AFM Scans and 3D topography. Shows picture of the 1 µm scan (left) and their respective modelled topography (right). Pictures of the scans provided by the microscope are compiled and analysed by Dr. Laura Charlton. 3D topography was modelled by Dr. Laura Charlton. **(A)** 'Untreated' is the negative control sample of just the PP film. **(B)** 'Pure HIS1' is the PP film treated with the purified HIS1 enzyme. **(C)** 'HIS1 Lysate' is the PP film treated with the HIS1 lysate. **(D)** 'Empty Vector Lysate' is the PP film treated with the empty vector (Li et al., 2018) lysate.

Fourier Transform Infrared Spectroscopy (FTIR)

Samples sent for FTIR study were treated with Pure HIS1 protein, HIS1 lysate, and EV lysate (Fig. 10). They were compared with negative control samples (HEPES-treated and Untreated) and $KMnO_4$-treated positive control samples. All samples shown in Figure 10 contained peaks distinctive of PP at around 2950 cm^{-1}, 2875 cm^{-1}, and 1375 cm^{-1} representing CH_3 asymmetric and symmetric bending, and around 2917 cm^{-1} and 2839 cm^{-1} for CH_2 asymmetric and symmetric bending ((Smith, 2024);Table S7). Negative controls showed expected results (Fig 10A; Fig. 10E; Fig. 10F). Oxidised $KMnO_4$ treated samples (Fig. 10B) displayed a large broad peak at 3200-3400 cm^{-1}, corresponding to O-H stretching vibrations, with a shoulder at 1550-1600 cm^{-1} corresponding to COO- bending (Fávaro et al., 2007). These distinctive oxidation absorptions are not observed on surfaces treated with pure HIS1 or HIS1 lysate (Fig. 10C, Fig. 10D), all of which are not notably different to untreated samples.

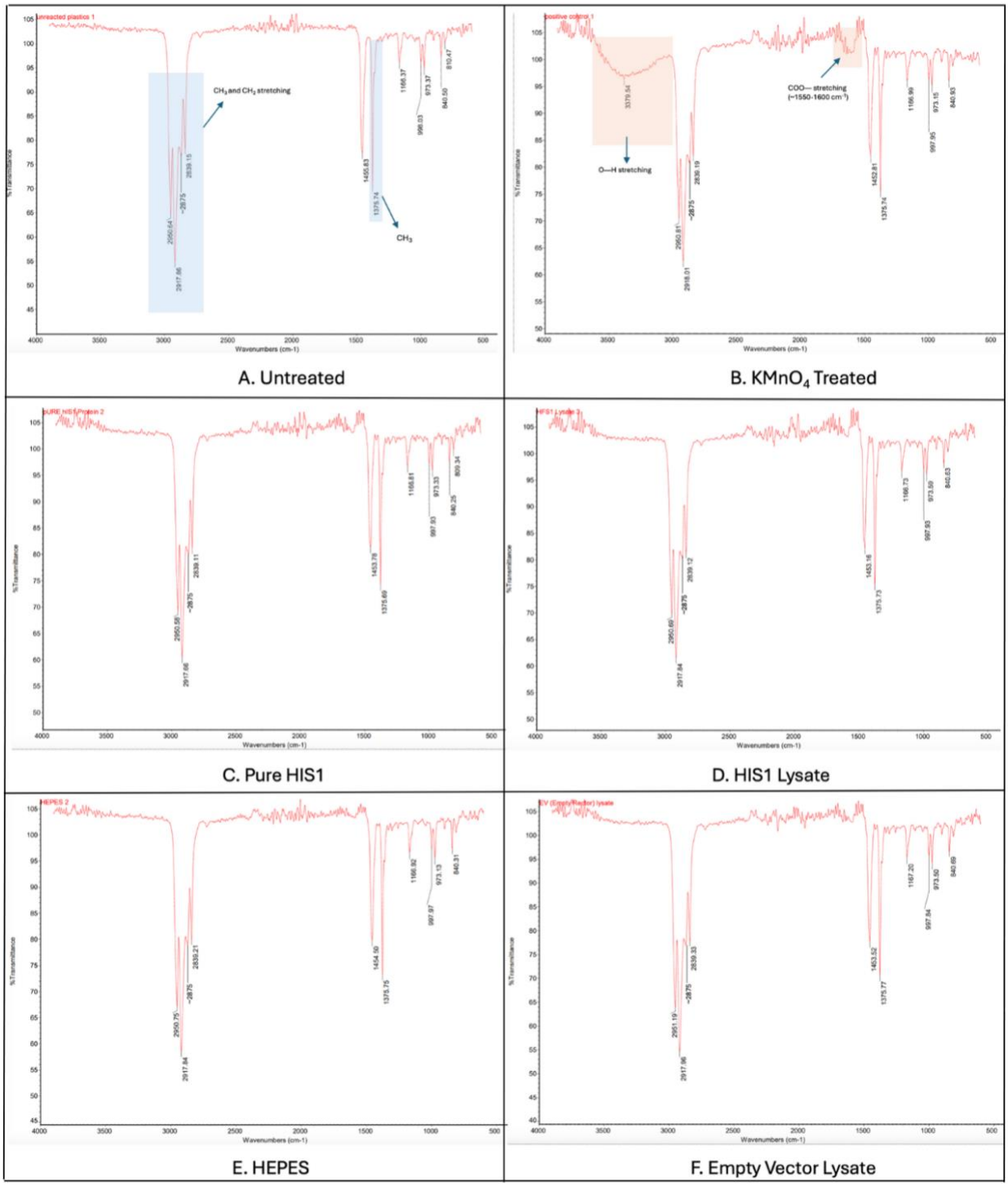

Figure 10. Infrared Spectra from FTIR Analysis of PP film surface. FTIR measurements and analysis was done by Cara Kane within Dr. Simone Dimartino's lab. **(A)** 'Untreated' is the negative control sample of just the PP film. **(B)** '$KMnO_4$-Treated' is the positive control sample of PP chemically oxidised by $KMnO_4$. **(C)** 'Pure HIS1' is the PP film treated with the purified HIS1 enzyme. **(D)** 'HIS1 Lysate' is the PP film treated with the HIS1 lysate. **(E)** 'HEPES' is the PP film treated in HEPES buffer. **(F)** 'Empty Vector Lysate' is the PP film treated with the empty vector (Li et al., 2018) lysate. Important peaks are annotated by coloured boxes. Blue indicates peaks characteristic of polypropylene, while orange indicates peaks characteristic of plastic oxidation.

High-Throughput Assay Development for Detection of Surface Oxidation of Polypropylene

In tandem with the DE of our PPase (HIS1), we attempted to develop a novel high-throughput assay for detection of surface oxidation. To our knowledge one is yet to be established in literature. Both assays rely on the specific binding of positively charged ions or dyes, which were later quantified calorimetrically. For proof of concept, both assays utilized PP 1.5ml microtubes treated with acidified $KMnO_4$ as positive controls (see methods). When transformed into a high-throughput assay, we utilised a PP 96-well plate treated with the same acidified $KMnO_4$ at varying times to test the sensitivity of our assay.

Toluidine Blue O

The TBO assay successfully differentiated between untreated and $KMnO_4$-treated polypropylene samples (Fig. 11B). Untreated polypropylene showed minimal TBO binding with an average absorbance of 0.08 ± 0.02 at 630nm, whilst the $KMnO_4$ samples demonstrated higher binding with an average absorbance of 1.61 ± 0.05. The difference between untreated and $KMnO_4$-treated samples was found to be statistically significant ($p=5.2 \times 10^{-7}$). The data represents an approximately 20-fold difference in absorbance between the two conditions and the difference in bound TBO was clearly visible by eye following desorption with SDS (Fig. 11C). Triplicates of microtubes were treated with HIS1 and EV lysates for TBO detection, however the data was not included due to issues with removal of a biological film that skewed absorbance readings even after repeated washes.

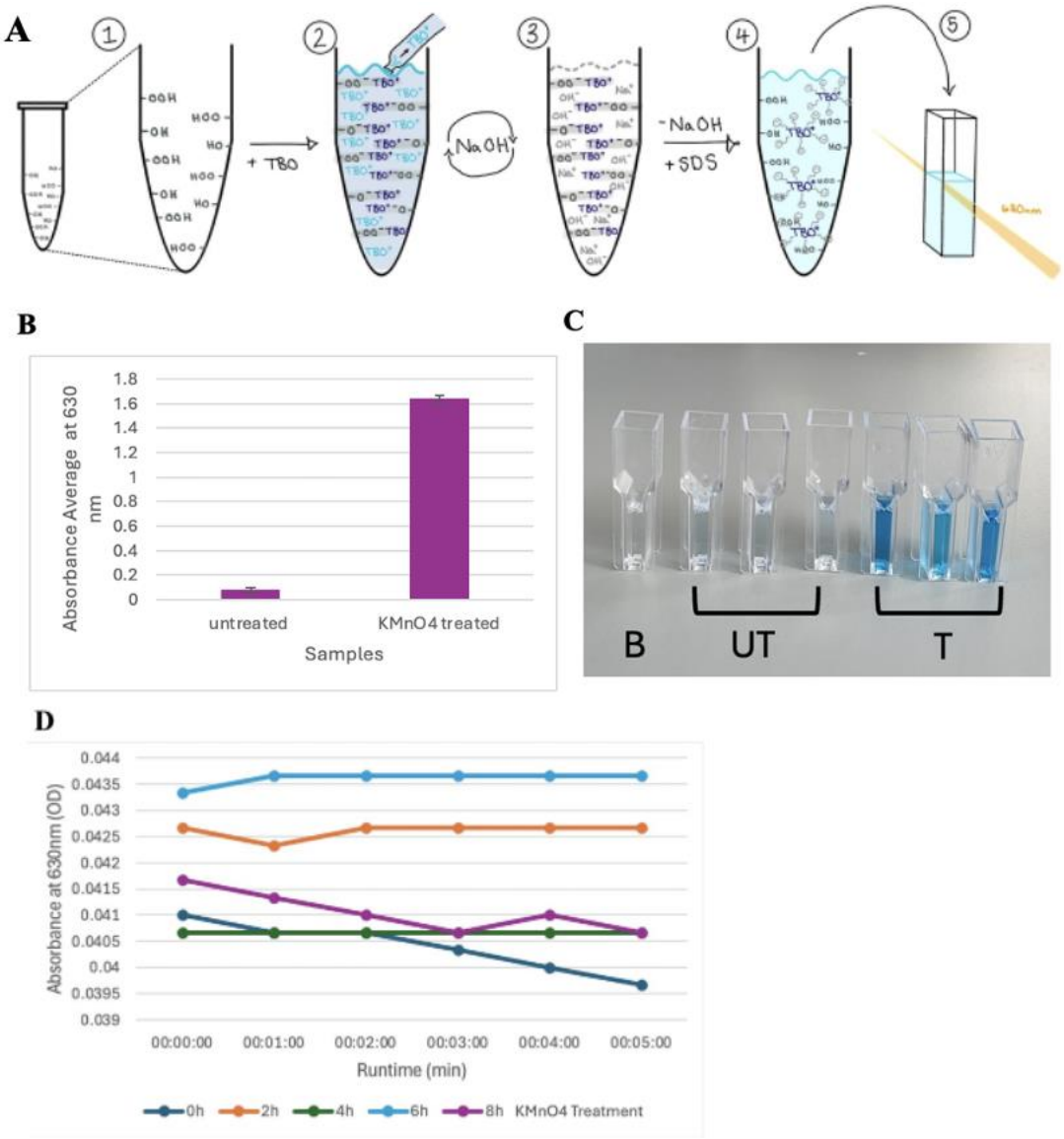

Figure 11. Development of Toluidine Blue O (TBO) Assay for Surface Oxidation Detection.

(A) Schematic Representation of TBO Assay for Detecting Polypropylene Oxidation**.** (1) Oxidised PP microtubes surface contain -COOH and -OH functional groups. (2) Known concentration of cationic TBO dye binds electrostatically to the oxidation groups on the microtube surface. (3) NaOH washing removes unbound TBO, leaving only dye specifically bound to oxidation groups. (4) SDS treatment desorbs bound TBO from the surface into solution. (5) Colorimetric quantification of desorbed TBO by absorbance measurement at 630nm. **(B)** Absorbance of TBO at 630 nm for Untreated and $KMnO_4$-treated PP microtubes. The microtubes were oxidised using the previously described $KMnO_4$ protocol for 8hr. Bars represent the mean absorbance values from three independent replicates. Error bars denote the population standard deviation. ($p=5.2 \times 10^{-7}$, two-tailed Welch's t-test, n=3). **(C)** Photographic Comparison of Cuvettes Containing TBO-treated PP Samples. UT= untreated polypropylene samples showing little to no blue colouration. T= 8hr $KMnO_4$-treated PP samples displaying visible blue colouration due to increased TBO binding to oxidised surface groups. B= SDS blank. **(D)** Testing sensitivity of TBO Assay in High Throughput Format on Polypropylene 96-Well Plate Treated with $KMnO_4$ at Varying Time Lengths**.** n=3. Wavelength = 630 nm. Absorbance readings were expected to increase with increasing time of $KMnO_4$ treatment.

This preliminary data demonstrates proof of concept, showing the TBO assay can distinguish between oxidised and untreated PP surfaces. To optimise the assay development, the 8hr $KMnO_4$ treatment should be repeated to verify results. The Minimum Detectable Change of 0.137 absorbance units was established by adding three times the standard deviation of untreated controls (3 × 0.01936 = 0.058) to the mean control value (0.079), ensuring confidence that any signal observed above this threshold indicates genuine oxidation rather than background noise. The oxidized sample absorbance of 1.639 exceeded this threshold by 12-fold, demonstrating the assay is sensitive to much lower oxidation levels. We then applied the assay to a 96-well format to test its ability to detect changes in PP oxidation in a high-throughput context. To test TBOs ability to detect varying amounts of oxidation, wells were treated with varying durations of KMnO4 treatment (Fig. 11D). An increase in absorbance from the 0hr to 8hr $KMnO_4$ treatment was expected, however no difference in absorbance was noted in any of the wells (Table S1). These results may be attributed to the decay of the TBO dye, as it was stored at room temperature in 1mM NaOH for a week, possibly affecting its binding capacity. The wells of the BIO-RAD PCR plates were made from virgin polypropylene which rules out any interference from surface treatments or coatings. This establishes that while the TBO assay successfully detects oxidation on microtubes, further optimisation is required for 96-well plate application for high-throughput screening.

Colorimetric quantification of surface carboxyl groups

Nickel (Ni^{2+})/Pyrocatechol Violet (PV)

Surface oxidation of PP was evaluated using the Ni^{2+}/PV assay adapted from (Hennig et al., 2011).In this assay, Ni^{2+} binds to surface carboxyl groups on oxidised PP, and residual unbound Ni^{2+} is quantified at 650 nm after complexation with PV (Fig. 12A). $KMnO_4$-treated PP served as the positive control, and untreated PP as the negative control. For PP microtubes, treated samples showed a ~25% lower absorbance than untreated samples (Fig. 12B), consistent with increased surface carboxylation. An unpaired t-test indicated significance (p=0.029), though Welch's correction yielded p=0.058, suggesting a

strong trend but not strictly significant. In contrast, PP films showed no difference between treated and untreated samples (Fig. 12B), possibly due to the sample size being too small (1.667mg).

To test the assay in a high-throughput format, 96-well PP plates (BIO-RAD PCR) were directly treated with $KMnO_4$ for 2–8 h. No significant absorbance differences were observed (Fig. 12C). Likely, due to limited assay sensitivity or unsuccessful $KMnO_4$ treatment as time constraints did not allow for verification of oxidation via FTIR analysis.

The Ni-PV colorimetric assay developed here showed an analytical limit of detection of ~13.7 μM Ni^{2+}, corresponding to ~0.0110 μmol·cm^{-2} of surface carboxyl groups (~66 groups·nm^{-2}) (Fig. S4). When variability in positive control PP samples was considered, the practical limit of detection rose to ~0.0641 μmol ·cm^{-2} (~386 groups·nm^{-2}) (Fig. S4). Although these limits of detection values are estimates due to the lack of triplicates in the calibration curve, they indicate that the assay can detect changes in oxidation equivalent to a few functional groups per square nanometer of surface. The assay was applied to test HIS1-mediated degradation; however, no detectable increase in surface carboxyl groups was observed. This suggests that any enzyme-driven oxidation was below the detection threshold, did not generate accessible carboxyl's, or that HIS1 was inactive under the conditions tested.

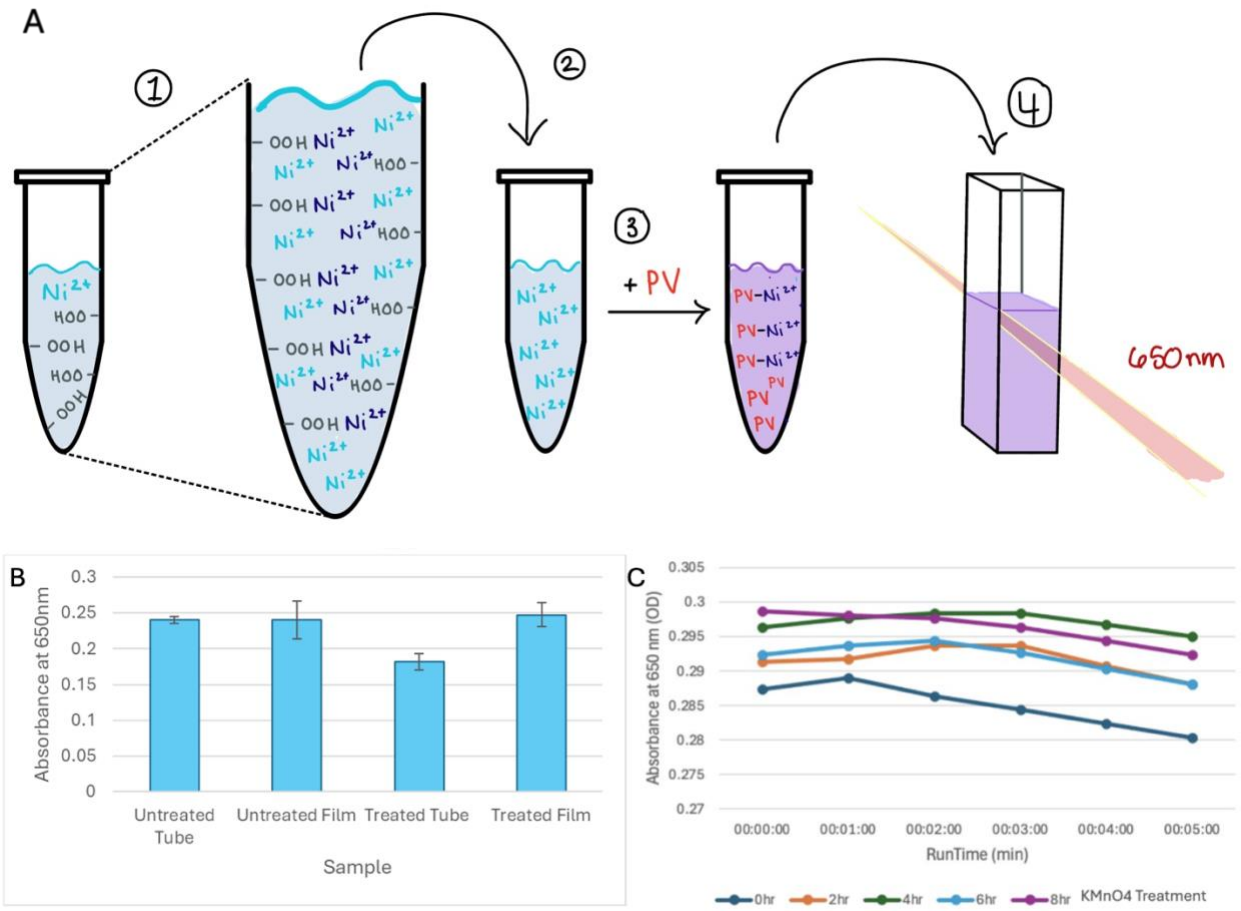

Figure 12: Development of Nickel-Pyrocatechol Violet (Ni^{2+} - PV) Assay for Surface Oxidation Detection. **(A)** *Schematic of the Ni^{2+} - PV colorimetric assay detecting surface carboxy groups on 1.5 ml polypropylene tubes.* 1) A known concentration of $NiCl_2$ (Ni^{2+}) is added to the oxidised PP tube. Ni^{2+} specifically binds in a 1:1 fashion to the surface carboxy groups. 2) The solution containing the unbound Ni^{2+} is then transferred into a fresh tube. 3) Pyrocatechol violet (orange/red in solution) is added to the Ni^{2+} solution. PV is purple when in complex with Ni^{2+}. 4) The solution is then transferred into a cuvette and absorbance is measured at 650nm. **(B)** *Absorbance readings from proof-of-concept Ni^{2+} - PV colorimetric assay for detection of surface carboxy groups on PP*. Untreated Tube (negative control, 1.5ml microtube) showed an average absorbance of 0.241 ± 0.005 (n=3), while untreated film (negative control, 1.667 mg hole-punched film) gave 0.248 ± 0.011 (n=3). Treated Tube (positive control) had an average absorbance of 0.182 ± 0.027 and treated film (positive control) showed 0.248 ± 0.014. *Error bars indicate standard deviation between triplicates.* Statistical analysis: untreated vs. treated tubes, un-paired t-test p=0.029 (Welch's correction, p=0.058); untreated vs treated films p>0.05. **(C)** *Absorbance readings from 96-well adaptation of the Ni^{2+} - PV assay.* The line plot indicates the plate readings at 650 nm for the wells treated with differing lengths of $KMnO_4$ treatment, n=3. Absorbance readings were expected to decrease with increasing time of treatment.

Discussion

Computational analyses revealed seven target sites for mutagenesis, showcasing that even with limited resources, molecular dynamics (MD) - guided screening can provide a semi-rational approach to DE. However, MD simulations were performed on a single representative frame rather than across an ensemble of conformations, likely reducing

predictive accuracy. Protein flexibility and full conformational landscapes of HIS1 were not captured, limiting the robustness of docking predictions(Karplus and McCammon, 2002); (Hollingsworth and Dror, 2018). Restricted computational power constrained both simulation length and sampling depth, factors known to bias residue prioritisation (Hospital et al., 2015). Future work could address these shortcomings through ensemble docking and computing clusters for enhanced computational power.

Experimentally, the mutagenesis strategy utilised the degenerate codon DTN at residue 110 as a proof of concept before expanding to additional sites. However, sequencing confirmed that no clones carried the intended DTN substitution, suggesting that although clean full-length PCR products were produced, the mutation was not incorporated. Site-saturation mutagenesis using degenerate codons frequently yields incomplete or skewed libraries, with certain codons absent or under-represented despite correct primer design (Li et al., 2018). Amplification bias in the megaprimer PCR step can favour recovery of parental sequences or over-represented codons (Sayous et al., 2020).Future work could employ library-wide quality control strategies to verify the incorporation of the intended mutation at the PCR product stage before transformation.

To assess HIS1 activity, multiple techniques were used. Initial TLC tests of purified HIS1 and HIS1 lysate showed no detectable activity, likely due to limited sensitivity (Fig. 6A, 6B). Future research should consider using HPLC, which had previously yielded positive results under similar conditions (Sadler Lab, unpublished data). In contrast, AFM analysis provided evidence for purified HIS1 activity, with a significant increase in surface roughness relative to negative controls (Fig. 8). HIS1 lysate showed no difference to negative controls, likely a result of low enzyme concentration or inactivity in given conditions (Fig. 8; Fig. 9). EV lysate samples showed protein coating particulates, underlying the need for improved washing protocols (Fig. S6). Additionally, using functionalised AFM tips and optimised measurement parameters would better represent real structural change. FTIR analysis detected distinct oxidation peaks following $KMnO_4$

treatment, validating it as a positive control. No oxidation peaks were detected following both HIS1 treatments, this can be attributed to the concentration of the oxidation groups being below the FTIR threshold of detection (3-5% of total) (Smith, 2024). Future optimisation of FTIR parameters and ATR accessories, along with performing internal triplicate scans could increase sensitivity and reproducibility in detecting HIS1-mediated surface oxidation.

We successfully adapted two colourimetric assays previously applied to non-PP plastics (Hennig et al., 2011, Yamamoto et al., 2023). Using both in parallel is advantageous: TBO provides a general readout of oxidative modifications, while Ni-PV offers specificity for carboxylation, enabling complimentary insights into the chemistry of surface oxidation. Both assays reliably detected oxidation in proof-of-concept experiments using $KMnO_4$-treated microtubes as positive controls (Fig. 11, Fig. 12).

In the context of HIS1 treatment, neither assay detected a measurable change in absorbance. This could reflect oxidation levels below detection thresholds, the absence of accessible carboxyl or hydroxyl groups generated by HIS1, or enzyme inactivity under the conditions tested. In 96-well plate trials, assay performance was inconsistent, possibly due to ineffective $KMnO_4$-treatment and limited time for optimisation of assay conditions at reduced volumes.

Future work should focus on verifying assay sensitivity across a range of PP oxidation states and fully optimising both methods for 96-well format. This would enable the development of a robust high-throughput screen suitable for DE studies, where mutant libraries of putative PPases such as HIS1 could be assessed for surface oxidation activity.

Materials and Methods:

In silico simulation of HIS1-substrate molecular docking for residue selection

To identify and prioritize hydrophobic mutation sites on HIS1 (PDB 8y4u), we first performed protein-only molecular dynamics (GROMACS; AMBER99SB-ILDN force field, TIP3P water) including energy minimization, 100 ps NVT, 100 ps NPT, and a 5 ns production run (Wang et al., 2024; Abraham et al., 2025; Lindahl et al., 2001). Trajectory quality was assessed by RMSD, RMSF, and radius of gyration, with equilibration achieved within ~1 ns. Per-residue solvent exposure was quantified using gmx sasa on a representative (final) frame to classify residues as exposed versus buried (threshold ~0.2 nm^2).

To map putative polymer-contacting patches, we constructed a polypropylene (PP) decamer (Open Babel) and performed docking with Autodock Vina using the final frame MD structure as a receptor and a search box encompassing the protein surface (Eberhardt et al., 2021, O'Boyle et al., 2011) (Trott and Olson, 2010). 20 poses were generated and residue–ligand contacts within 4–6 Å across poses were further analyzed. Candidate residues were refined by excluding positions within ~6 Å of cofactors (Fe^{2+}, 2-oxoglutarate; positions identified by alignment to cofactor-bound HIS1, PDB: 8s7b), buried residues (low SASA), and highly flexible positions (RMSF threshold ~0.25 nm). The resulting shortlist was evaluated with FoldX to compute the average ΔΔG per hydrophobic substitution at each site (Delgado et al., 2019). Residues were subsequently ranked by mutational stability.

Sub-cloning and Expression of HIS1

Escherichia coli BL21(DE3) with pET28-A plasmid containing the HIS1 gene was inoculated from a glycerol stock acquired from Dr. Johanna Sandler's lab into 5mL of LB containing 5µL of kanamycin. Then, the stock was incubated overnight at 200 rpm in 37°C. 2mL of overnight culture was added to 200mL of TB with 200 µL of kanamycin then incubated at 180 rpm in 30°C until absorbance at 600nm reached 0.8-0.9. The flasks were then incubated on ice for 20 minutes. Co-factors were added at 2mM FeSO4 and 6mM 2-oxoglutarate, then the reaction mixture was induced with 0.4 mM IPTG. Induced cultures were incubated at 200 rpm in 20°C for 20 hours. Cells were harvested by centrifugation at

10000 xg, 4°C for 20 min and supernatant was discarded. Cell pellets were stored in the –20°C freezer.

Mutant Library Synthesis

Two-phase Mutagenesis Strategy

Through computational analyses, we identified seven residues (110, 148, 268, 297, 304, 305, 307) to mutate using the degenerate codon DTN. We planned a two-phase mutagenesis strategy to minimize library size; due to a delay in screen optimization, this step was ultimately deferred.

Vector Amplification

pET28-A vectors used for HIS1 expression were cloned and purified using a QIAprep Spin Miniprep kit. Plasmid samples were then digested using 1µL of EcoRI and HindIII for 1 hour. Vector backbone samples were analysed and gel extracted via 0.8% agarose gel to verify band length; DNA concentration was measured using a Nanodrop spectrophotometer.

Site-directed mutagenesis

Two approaches were tested to generate single-site mutants: degenerate codon substitution via Bsa1 sites, and library synthesis using mutant megaprimers. All primers used are listed in Table 1. All PCRs were conducted using the Q5®High-Fidelity DNA Polymerase (M0491) standard protocol in 50µL reaction tubes unless otherwise stated.

Degenerate Codon Substitution via Bsa1 Sites

Primers PPase_Fs and PPase_Rs from Table 1 were used to generate single site mutants for residue 110. Samples were electrophoresed on 0.8% agarose gels, but no visible bands were observed. After several rounds of optimization, this strategy was discontinued in favour of the mutant megaprimers, as this strategy would facilitate both single-site and combinatorial mutagenesis.

Mutant Megaprimers

Non-mutagenic and mutagenic primers were designed following a protocol by the Sadler Lab (Sadler et al., 2018)Table 1 highlights all primers used in this step; crucially, the degenerate codon DTN in the mutagenic forward primers were flanked by sequences with a T_m of 60℃. Asymmetric PCRs were conducted with a 100:1 primer concentration, with

the final concentrations for the non-mutagenic reverse primer and mutagenic forwards primers being 2500nM and 25nM respectively. An annealing temperature of 65℃ was set for 35 cycles (Table S.11). Symmetric PCRs consisting of equal primer concentrations were set up for each asymmetric PCR as a positive control. Single-stranded PCR products were analyzed via 0.8% or 2% agarose gels based on expected band size. 1µL Dpn1 digests were conducted on the product to remove residual template DNA, followed by purification using a Promega Wizard® SV Gel and PCR Clean-Up System. Mutant megaprimers were concentrated by pooling 6 50µL reactions at the purification stage. DNA concentrations were measured using a Nanodrop spectrophotometer.

Full-length gene products were generated using mutant megaprimers as a reverse primer. Reactions were performed based on the measured concentration of the single-stranded mutant megaprimer samples. Aliquots of full-length PCR products were visualized on 0.8% agarose gels to confirm correct band size, before digestion with 1µL EcoRI and HindIII for 1 hour. The product was then purified using a Promega Wizard® SV Gel and PCR Clean-Up System kit and Nanodropped to measure DNA concentration.

***Table 1: Primer sequences for mutant library synthesis*.**

Purpose	Primer name	Primer sequence
Cloning (non-mutagenic)	PPase_F	ACTGGAATTCCCTGGTGCCACGCG
	PPase_R	CTAAATACGCAGGCTATCAATATAGCGTTC
Combinatorial mutagenesis	PPase_110_F	CGCAAACAGAAATTCAGCdtnCTGATCGATGGCAAGAAC
	PPase_148_F	CGTGTGGAACCGAAAdtnGAACAGGATCTGGCATTTTG
	PPase_268_F	CTGCTGATTAATCTGGGTdtnACAATGGAAGTTATGTGC
	PPase_297_F	GAAAAAGAACGTATTAGCCTGdtnATGCTGTATAGCGTGAATG
	PPase_304_F	CAATGCTGTATAGCGTGAATdtnGAGAAAGATATTGAACCTGCC
	PPase_305_F	GCTGTATAGCGTGAATGATdtnAAAGATATTGAACCTGCCG
	PPase_307_F	GTATAGCGTGAATGATGAGAAAdtnATTGAACCTGCCGC

Single-site mutagenesis	PPase_Fs	atcGGTCTCttcagcdtnCTGATCGATGGCAAGAACTTT
	PPase_Rs	ATCggtctcGCTGAATTTCTGTTTGCGTTC

Sequencing

Ligation and Transformation

Ligation reactions were performed in 20µL reactions using T4 DNA ligase (Table S.12). Separate reactions without the DNA insert (+L-I) and without the ligase or the insert (-L-I) were set up as controls. Each reaction tube was mixed gently then incubated at room temperature for 1 hour.

10µL from each ligation reaction was then mixed with 100µL of competent cells transformation. Two more controls were set up at this stage: a positive control consisting of 50µL of competent cells and 1µL of the template plasmid DNA, and a negative control with 50µL of competent cells. These samples were incubated on ice for 15 minutes, heat-shocked at 42℃ for 1 minute, then returned to ice for 1 minute. 250µL of SOC was added to the samples before incubation at 37℃ for 1 hour. 50µL aliquots of each sample were plated onto LB agar plates, then incubated at 37℃ overnight.

Sanger Sequencing

6 colonies from the +L+I plates were sent for Sanger sequencing prior to screening to verify mutations at the target site. PPase_F and PPase_R were used at sequencing primers (Table 1).

Chemicals used in Protein Purification

Lysis buffer was made up with 20mM Tris-HCl, 100mM NaCl, 2.5mM $MgCl_2$, and 0.5 mM $CaCl_2$d. Binding buffer was made up with 20mM Tris-HCl and 0.1 mM $MgCl_2$. Wash buffer was made up with 20mM Tris-HCl, 10mM Imidazole, 200mM NaCl, and 0.1mM $MgCl_2$. Elution buffer was made up of 20mM Tris-HCl, 500mM Imidazole, 50mM NaCl, and 0.1mM $MgCl_2$. The column wash buffer was made up of 20mM Tris-HCl and 500 mM imidazole.

HIS-1 Protein Purification

After protein expression, the cell pellets were resuspended in 20mL of BugBuster® and incubated for 30 minutes at room temperature. The BugBuster® solution was centrifuged at 40,000 xg for 30 minutes at 4°C. The lysate supernatant was kept as the soluble lysate product and the pellet was discarded.

Ni-sepharose column was obtained from Dr. Johanna Sandler's lab. The Ni-sepharose column was washed with 30 mL of MilliQ water and equilibrated with 30 mL of binding buffer. The prepared lysate was loaded into the column and the flow-through was collected. Then the column was washed with 10mL of washing buffer until the absorbance was close to 0. The column was then eluted with 1mL of elution buffer until the absorbance was close to 0. Elutions with the highest absorbances were pooled together and concentration of protein calculated from the pooled elution absorbance. Samples at all purification points were taken for SDS PAGE analysis. Columns were then washed with 20mM tris, 500mM imidazole at pH 8, ran through with MilliQ then 20% ethanol for storage. Three washes were done.

A Vivaspin® column was soaked overnight. Using the Vivaspin® column, the entirety of the pooled elution was spun down to 0.5 ml or less in a centrifuge at max speed. Flow through was discarded. Concentrated protein was resuspended in HEPES and spun down repeatedly until imidazole concentration was estimated to be 3mM or less.

Degradation of polypropylene

After expression, the cells were lysed in BugBuster® for 30 minutes at room temperature, then centrifuged at 40,000 xg for 30 minutes at 4 degrees. Pellet was discarded and the supernatant was incubated with 5mg polypropylene at pH7 in 30°C with 2mM $FeSO_4$ and 6 mM 2-oxoglutarate. Enzyme solution and its cofactors were exchanged every 24 hours.

KMnO4 treatment of polypropylene

Plastics were oxidised using acidified potassium permanganate as described previously by Fávaro et al., (2007), with minor modifications. A 96-well plate, polypropylene films in microtubes, and empty polypropylene microtubes were ultrasonically cleaned with

acetone and ethanol, then dried at 50 °C for 1 h. Each sample was treated with 0.5 M HCl/0.25 M $KMnO_4$ and incubated at 45 °C for 2, 4, 6, or 8 h. Following treatment, samples were rinsed repeatedly with water until colourless to remove residual $KMnO_4$. Any MnO_2 reaction by-product deposits on the plastic surface were removed with a 12 M HCl rinse.

Colorimetric quantification of surface carboxyl groups using pyrocatechol violet and nickel-(2+) ions

Surface oxidation of PP was quantified using a colorimetric assay adapted from Hennig et al (2011). This method relies on the specific binding of Ni^{2+} to surface carboxyl groups, and residual Ni^{2+} in the supernatant was quantified spectrophotometrically in a complex with Pyrocatechol violet (PV).

Controls: we used $KMnO_4$/HCl oxidized PP as our positive controls and untreated PP as our negative controls.

During the stages of optimisation, the appropriate concentrations of Ni^{2+} for our spectrometer were deciphered using 40uM of PV. PP fibres were initially used to decipher a suitable sample input volume (10-100uL slurry). Next components in the lysate degradation mix were found to interact with either Ni^{2+} or PV. To address this, all the treated samples were rinsed thoroughly with 10mM HEPEs (pH 7) before the assay.

The final protocol: Plastics were incubated in 10mM HEPEs and 400uM Ni^{2+}, incubated at 25ºC for 2 minutes and the liquid was transferred to a fresh well or tube. PV was added (final concentration of 40uM) and absorbance was measured at 650nm immediately after.

The assay was also adapted to be conducted with $KMnO_4$-treated 96-well polypropylene Hard-Shell PCR plates (Bio-Rad) instead of microtubes. All protocol steps were kept the same; for absorbance readings the solutions were transferred to a flat bottom 96 well plate suitable for the plate reader.

Equations used to calculate sensitivity (LOD and LOQ)

$$LOD_{[Ni]} = \frac{3.3 \times s_{blank}}{m},\ LOQ_{[Ni]} = \frac{10 \times s_{blank}}{m}$$

$m = gradient\ of\ the\ calibration\ curve$ (Fig. S3A)

$s_{blank} = SD\ of\ blank\ (negative\ control)\ absorbance\ readings$ (Fig. S3C)

Toluidine Blue O staining for quantification of surface organic compounds

Polypropylene microtubes were used for the TBO assay which was adapted from Yamamoto et al. (2023). The microtubes were treated with HEPES buffer with HIS1 enzymatic cofactors, Empty Vector lysate reaction solution, HIS1 lysate reaction solution, and pure HIS1 enzyme reaction solution at 30°C for 48 hours. The reaction tubes were ultrasonically cleaned with 1% SDS, distilled water, and 75% ethanol for 5 minutes then dried at ~50 °C for 1 h.

The samples were incubated in 0.1% TBO in 1mM NaOH at 40 °C for 15 min, shaking at 250 rpm. The samples were then washed with 1mM NaOH at 40 °C for 5 min, shaking at 250 rpm. This wash step was repeated until the supernatant was clear, around 4 times, or until absorbance was close to 0. TBO bound to surface of the sample was then desorbed via incubation in 20% SDS solution at 40 °C for 30 minutes, shaking at 250 rpm. The absorbance of desorbed SDS supernatant was measured at 630nm and the concentration of TBO bound to polypropylene surface was calculated.

The assay was also adapted to be conducted with $KMnO_4$-treated 96-well polypropylene Hard-Shell PCR plates (Bio-Rad) instead of microtubes. All the dye and wash steps were kept the same; for absorbance readings the SDS solutions were transferred to a flat bottom 96 well plate suitable for the plate reader.

Surface Contact Angle (SCA)

Preparation protocols for SCA was taken from (Bae et al., 2022). Black polypropylene pieces (7mm width, 28mm height, 2mm thickness) were washed with 70% ethanol and water and dried at 55 °C for 1h before the day 0 surface contact angle measurements were taken using a drop shape analyser. Three points were analysed along each plastic piece and the drop size used was 7ul. The software was run for 2 minutes for each water drop with a data point taken every 2 seconds. Three plastics were treated with HIS1 and three with EV in 2ml microtubes overnight. Separately three plastics were treated with $KMnO_4$ for 4h and three for 8h. All treated plastics were cleaned the following day using 1:10 IPA and

water in a sonicating water bath for 3 minutes, then washed with 70% ethanol and water and dried at 55 °C for 1h. All plastics were then re-analysed with the drop shape analyser. The plastics were treated with HIS1 and EV for five days with the reaction mixture exchanged every 24h and surface contact angle measurements taken each day. No further treatment was done to the $KMnO_4$-treated plastics.

FTIR

Clear square polypropylene films of 1cm x 1cm sizes were used for FTIR. They were cleaned in a sonicating water bath with 1% SDS, distilled water, and 75% ethanol for 5 minutes then dried at 50 °C for 1 h. FTIR analysis was done in collaboration with Dr. Simone Dimartino's lab by Ms. Cara Kane in the School of Engineering under Bioengineering.

AFM

Clear circular polypropylene films with diameters of 6mm were used for AFM. Samples sent for AFM study (1 µm and 10 µm scales) were treated with HEPES buffer, Pure HIS1 protein, HIS1 lysate, and EV lysate. They were compared with untreated and HEPES buffer treated samples (negative control). Samples were then ultrasonically cleaned with 1% SDS, distilled water, and 75% ethanol for 5 minutes then dried at 50 °C for 1 h. AFM analysis was done in collaboration with Dr. Laura Charlton at the Centre for Science at Extreme Conditions. Scanning speed was at 1.0 Hz, with resolution of 256*256 pixels. Thickness and roughness values were acquired.

GC-MS

Clear 5mg polypropylene films were treated with purified HIS1 for 72h with the reaction mixture collected and stored at 4 degrees and subsequently replaced every 24h. The same was done with HEPES for our negative control. The stored reaction mixtures for HIS1 and HEPES were pooled together to form two samples. 3:1 chilled HPLC-grade methanol was

added to the samples and incubated for 30 minutes on ice. Samples were centrifuged at 12,000 rpm at 4 °C for 30 minutes. Supernatants were collected and sent to the Waddington building where GC-MS was performed in collaboration with Dr Tessa Moses at EdinOmics. In preparation for GC-MS analysis 10% dichloromethane was added to the samples. 1µl of the samples were injected into a DB-5ms 40m x 250 µm x 0.25 µm GC column for analysis. Sample components were separated using a helium flow rate of 1 mL/min and fragmentation patterns were obtained with 70eV electron energy. The obtained chromatograms were interrogated for differential peaks and their mass spectra searched against NIST library to assign chemical identity.

TLC analysis of HPP breakdown by HIS1 lysate and purified HIS1

Reaction mixtures were prepared to assess the activity of HIS1 on 4-hydroxyphenypyruvate (HPP). Each 300µl reaction contained 2mM $FeSO_4$, 6mM (Li et al, 2018). The reactions also contained 6mM HPP, while control reactions were set up without HPP. Reactions we incubated at 30^{o}C for 24 h. Additionally, a reaction mixture was set up with 0.5mg/ml pure HIS1.

Following incubation, reaction products were analysed by thin-layer chromatography (TLC). Samples of the reaction mixtures were spotted in triplicate onto silica gel TLC plates and ran using a solvent of ethyl acetate:hexane:acetic acid (70:30:2). Plates were air-dried, and the migration of HPP and potential breakdown products was visualised under UV light.

ACKNOWLEDGEMENTS

We thank our primary supervisor Dr. Heather Barker for her invaluable mentorship and support throughout this project. We also thank Dr. Medoune Sarr for his continuous guidance and contributions. We are grateful to our supervisors Prof. Chris French, Dr. Joanna Sadler, and Dr. Nadanai Laohakunakorn for their support throughout the project. We acknowledge Dr. Tessa Moses (EdinOmics) for GC-MS analysis, Dr. Laura Charlton for AFM measurements and analysis, Cara Kane for FTIR analysis, and Dr. Andreia Fonseca Da Silva for access to the Drop Shape Analyser. We are grateful to Hayley Patterson for her

dedicated daily support in the laboratory, and to Dr. David Hills for his assistance. Rick Miyamoto would like to thank his girlfriend, Elizabeth Lau, for the support and all the lunches she's made him. Lastly, we would like to acknowledge the nights the team spent cooking and talking at dinners; from this project, if nothing else, we each came out with 4 more friends.

BIBLIOGRAPHY

ABRAHAM, M., ALEKSEENKO, A., ANDREWS, B., BASOV, V., BAUER, P., BIRD, H., BRIAND, E., et al., 2025. GROMACS 2025.3 Manual. Version 2025.3. [software documentation] Zenodo. Available at: https://doi.org/10.5281/zenodo.16992569 [Accessed 29 Sep. 2025].

BAE, G., PARK, T. & SONG, I. H. 2022. Surface Modification of Polymethylmethacrylate (PMMA) by Ultraviolet (UV) Irradiation and IPA Rinsing. *Micromachines,* 13**,** 9. DOI: 10.3390/mi13111952

BUSS, O., RUDAT, J. & OCHSENREITHER, K. 2018. FoldX as Protein Engineering Tool: Better Than Random Based Approaches? *Computational and Structural Biotechnology Journal,* 16**,** 25-33. Available at: https://doi.org/10.1016/j.csbj.2018.01.002

DELGADO, J., RADUSKY, L. G., CIANFERONI, D. & SERRANO, L. 2019. FoldX 5.0: working with RNA, small molecules and a new graphical interface. *Bioinformatics,* 35**,** 4168-4169. DOI: 10.1093/bioinformatics/btz184

EBERHARDT, J., SANTOS-MARTINS, D., TILLACK, A. F. & FORLI, S. 2021. AutoDock Vina 1.2.0: New Docking Methods, Expanded Force Field, and Python Bindings. *Journal of Chemical Information and Modeling,* 61**,** 3891-3898. DOI: 10.1021/acs.jcim.1c00203

FáVARO, S. L., RUBIRA, A. F., MUNIZ, E. C. & RADOVANOVIC, E. 2007. Surface modification of HDPE, PP, and PET films with KMnO4/HCl solutions. *Polymer Degradation and Stability,* 92**,** 1219-1226. Available at: https://doi.org/10.1016/j.polymdegradstab.2007.04.005

GEWERT, B., PLASSMANN, M. M. & MACLEOD, M. 2015. Pathways for degradation of plastic polymers floating in the marine environment. Environmental Science-Processes & Impacts, 17, 1513-1521. Available at: DOI:https://doi.org/10.1039/C5EM00207A

GEYER, R., JAMBECK, J. R. & LAW, K. L. 2017. Production, use, and fate of all plastics ever made. *Science Advances,* 3**,** 5. DOI: 10.1126/sciadv.1700782

HENNIG, A., HOFFMANN, A., BORCHERDING, H., THIELE, T., SCHEDLER, U. & RESCH-GENGER, U. 2011. Simple Colorimetric Method for Quantification of Surface Carboxy Groups on Polymer Particles. *Analytical Chemistry,* 83**,** 4970-4974. Available at: https://doi.org/10.1021/ac2007619

HOLLINGSWORTH, S. A. & DROR, R. O. 2018. Molecular Dynamics Simulation for All. *Neuron,* 99**,** 1129-1143. DOI: 10.1016/j.neuron.2018.08.011

KARPLUS, M. & MCCAMMON, J. A. 2002. Molecular dynamics simulations of biomolecules (vol 9, pg 646, 2002). *Nature Structural Biology,* 9**,** 788-788. DOI: 10.1038/nsb0902-646

LI, A. T., ACEVEDO-ROCHA, C. G. & REETZ, M. T. 2018. Boosting the efficiency of site-saturation mutagenesis for a difficult-to-randomize gene by a two-step PCR strategy.

Applied Microbiology and Biotechnology, 102**,** 6095-6103. DOI: 10.1007/s00253-018-9041-2

LINDAHL, E., HESS, B. & VAN DER SPOEL, D. 2001. GROMACS 3.0: a package for molecular simulation and trajectory analysis. *Journal of Molecular Modeling,* 7**,** 306-317. Available at: https://doi.org/10.1007/s008940100045

Maeda, H., Murata, K., Sakuma, N., Takei, S., Yamazaki, A., Karim, M. R., Kawata, M., Hirose, S., Kawagishi-Kobayashi, M., Taniguchi, Y., Suzuki, S., Sekino, K., Ohshima, M., Kato, H., Yoshida, H., & Tozawa, Y. (2019). A rice gene that confers broad-spectrum resistance to β-triketone herbicides. *Science*. https://doi.org/aax0379

MARTINEZ, S. & HAUSINGER, R. P. 2015. Catalytic Mechanisms of Fe(II)-and 2-Oxoglutarate-dependent Oxygenases. *Journal of Biological Chemistry,* 290**,** 20702-20711. DOI: 10.1074/jbc.R115.648691

NORDAHL, S. L., BARAL, N. R., HELMS, B. A. & SCOWN, C. D. 2023. Complementary roles for mechanical and solvent- based recycling in low- carbon, circular polypropylene. *Proceedings of the National Academy of Sciences of the United States of America,* 120**,** 8. DOI: 10.1073/pnas.2306902120

O'BOYLE, N. M., BANCK, M., JAMES, C. A., MORLEY, C., VANDERMEERSCH, T. & HUTCHISON, G. R. 2011. Open Babel: An open chemical toolbox. *Journal of Cheminformatics,* 3**,** 14. DOI: 10.1186/1758-2946-3-33

SADLER, J. C., GREEN, L., SWAINSTON, N., KELL, D. B. & CURRIN, A. 2018. Fast and Flexible Synthesis of Combinatorial Libraries for Directed Evolution. *In:* SCRUTTON, N.

(ed.) *Enzymes in Synthetic Biology*. San Diego: Elsevier Academic Press Inc. DOI: 10.1016/bs.mie.2018.04.006

SAYOUS, V., LUBRANO, P., LI, Y. Y. & ACEVEDO-ROCHA, C. G. 2020. Unbiased libraries in protein directed evolution. *Biochimica Et Biophysica Acta-Proteins and Proteomics,* 1868**,** 11. DOI: 10.1016/j.bbapap.2019.140321

SMITH, B. C. 2024. Infrared Spectral Interpretation, In The Beginning I: The Meaning of Peak Positions, Heights, and Widths. *Spectroscopy,* 39**,** 36. DOI: 10.56530/spectroscopy.fi6379n1

TAN, Q. L., CHEN, W. T., LIU, H., YAN, W. D., HUANG, X. & LI, Y. 2024. The programmed sequence-based oxygenase screening for polypropylene degradation. *Journal of Hazardous Materials,* 465**,** 9. DOI: 10.1016/j.jhazmat.2023.133173

Trott, O. and Olson, A.J., 2010. AutoDock Vina: Improving the speed and accuracy of docking with a new scoring function, efficient optimization, and multithreading. *Journal of Computational Chemistry*, 31(2), pp.455–461. https://doi.org/10.1002/jcc.21334.

WANG, N., HE, S. B., YANG, B. B., ZHANG, H., LIU, D. D., SONG, P. F., CHEN, T. T., WANG, W. Q., GE, H. H. & MA, J. M. 2024. Crystal structure of HPPD inhibitor sensitive protein from Oryza sativa. *Biochemical and Biophysical Research Communications,* 704**,** 5. DOI: 10.1016/j.bbrc.2024.149672

WANG, Y. J., XUE, P., CAO, M. F., YU, T. H., LANE, S. T. & ZHAO, H. M. 2021. Directed Evolution: Methodologies and Applications. *Chemical Reviews,* 121**,** 12384-12444. DOI: 10.1021/acs.chemrev.1c00260

YAMAMOTO, K., ASAHARA, H., HARADA, K., ITABASHI, Y., OHKUBO, K. & INOUE, T. 2023. One-step antibacterial modification of polypropylene non-woven fabrics via oxidation

using photo-activated chlorine dioxide radicals. *Journal of Materials Chemistry B,* 11**,** 5101-5107. doi.org/10.1039/D3TB00586K

BAE, G., PARK, T. & SONG, I. H. 2022. Surface Modification of Polymethylmethacrylate (PMMA) by Ultraviolet (UV) Irradiation and IPA Rinsing. *Micromachines,* 13**,** 9.

BUSS, O., RUDAT, J. & OCHSENREITHER, K. 2018. FoldX as Protein Engineering Tool: Better Than Random Based Approaches? *Computational and Structural Biotechnology Journal,* 16**,** 25-33.

DELGADO, J., RADUSKY, L. G., CIANFERONI, D. & SERRANO, L. 2019. FoldX 5.0: working with RNA, small molecules and a new graphical interface. *Bioinformatics,* 35**,** 4168-4169.

EBERHARDT, J., SANTOS-MARTINS, D., TILLACK, A. F. & FORLI, S. 2021. AutoDock Vina 1.2.0: New Docking Methods, Expanded Force Field, and Python Bindings. *Journal of Chemical Information and Modeling,* 61**,** 3891-3898.

FáVARO, S. L., RUBIRA, A. F., MUNIZ, E. C. & RADOVANOVIC, E. 2007. Surface modification of HDPE, PP, and PET films with KMnO4/HCl solutions. *Polymer Degradation and Stability,* 92**,** 1219-1226.

GEWERT, B., PLASSMANN, M. M. & MACLEOD, M. 2015. Pathways for degradation of plastic polymers floating in the marine environment. *Environmental Science-Processes & Impacts,* 17**,** 1513-1521.

GEYER, R., JAMBECK, J. R. & LAW, K. L. 2017. Production, use, and fate of all plastics ever made. *Science Advances,* 3**,** 5.

HENNIG, A., HOFFMANN, A., BORCHERDING, H., THIELE, T., SCHEDLER, U. & RESCH-GENGER, U. 2011. Simple Colorimetric Method for Quantification of Surface Carboxy Groups on Polymer Particles. *Analytical Chemistry,* 83**,** 4970-4974.

HOLLINGSWORTH, S. A. & DROR, R. O. 2018. Molecular Dynamics Simulation for All. *Neuron,* 99**,** 1129-1143.

KARPLUS, M. & MCCAMMON, J. A. 2002. Molecular dynamics simulations of biomolecules (vol 9, pg 646, 2002). *Nature Structural Biology,* 9**,** 788-788.

LI, A. T., ACEVEDO-ROCHA, C. G. & REETZ, M. T. 2018. Boosting the efficiency of site-saturation mutagenesis for a difficult-to-randomize gene by a two-step PCR strategy. *Applied Microbiology and Biotechnology,* 102**,** 6095-6103.

MARTINEZ, S. & HAUSINGER, R. P. 2015. Catalytic Mechanisms of Fe(II)-and 2-Oxoglutarate-dependent Oxygenases. *Journal of Biological Chemistry,* 290**,** 20702-20711.

NORDAHL, S. L., BARAL, N. R., HELMS, B. A. & SCOWN, C. D. 2023. Complementary roles for mechanical and solvent- based recycling in low- carbon, circular polypropylene. *Proceedings of the National Academy of Sciences of the United States of America,* 120**,** 8.

O'BOYLE, N. M., BANCK, M., JAMES, C. A., MORLEY, C., VANDERMEERSCH, T. & HUTCHISON, G. R. 2011. Open Babel: An open chemical toolbox. *Journal of Cheminformatics,* 3**,** 14.

SADLER, J. C., GREEN, L., SWAINSTON, N., KELL, D. B. & CURRIN, A. 2018. Fast and Flexible Synthesis of Combinatorial Libraries for Directed Evolution. *In:* SCRUTTON, N. (ed.) *Enzymes in Synthetic Biology*. San Diego: Elsevier Academic Press Inc.

SAYOUS, V., LUBRANO, P., LI, Y. Y. & ACEVEDO-ROCHA, C. G. 2020. Unbiased libraries in protein directed evolution. *Biochimica Et Biophysica Acta-Proteins and Proteomics,* 1868**,** 11.

SMITH, B. C. 2024. Infrared Spectral Interpretation, In The Beginning I: The Meaning of Peak Positions, Heights, and Widths. *Spectroscopy,* 39**,** 36.

WANG, N., HE, S. B., YANG, B. B., ZHANG, H., LIU, D. D., SONG, P. F., CHEN, T. T., WANG, W. Q., GE, H. H. & MA, J. M. 2024. Crystal structure of HPPD inhibitor sensitive protein from Oryza sativa. *Biochemical and Biophysical Research Communications,* 704**,** 5.

WANG, Y. J., XUE, P., CAO, M. F., YU, T. H., LANE, S. T. & ZHAO, H. M. 2021. Directed Evolution: Methodologies and Applications. *Chemical Reviews,* 121**,** 12384-12444.

YAMAMOTO, K., ASAHARA, H., HARADA, K., ITABASHI, Y., OHKUBO, K. & INOUE, T. 2023. One-step antibacterial modification of polypropylene non-woven fabrics via oxidation using photo-activated chlorine dioxide radicals. *Journal of Materials Chemistry B,* 11**,** 5101-5107.